Finer discrimination of brain activation with local multivariate distance*

Zhen Zonglei, Tian Jie** and Zhang Hui

(Medical Image Processing Group, Key Laboratory of Complex Systems and Intelligence Science, Institute of Automation, Chinese Academy of Sciences, Beijing 100080, China)

Accepted on June 12, 2007

Abstract The organization of human brain function is diverse on different spatial scales. Various cognitive states are always represented as distinct activity patterns across the specific brain region on fine scales. Conventional univariate analysis of functional MRI data seeks to determine how a particular cognitive state is encoded in brain activity by analyzing each voxel separately without considering the fine-scale patterns information contained in the local brain regions. In this paper, a local multivariate distance mapping (LMDM) technique is proposed to detect the brain activation and to map the fine-scale brain activity patterns. LMDM directly represents the local brain activity with the patterns across multiple voxels rather than individual voxels, and it employs the multivariate distance between different patterns to discriminate the brain state on fine scales. Experiments with simulated and real fMRI data demonstrate that LMDM technique can dramatically increase the sensitivity of the detection for the fine-scale brain activity patterns which contain the subtle information of the experimental conditions.

Keywords: functional magnetic resonance imaging (fMRI), statistical analysis, multivariate distance, local pattern, pattern classification.

Functional magnetic resonance imaging (fMRI) has become a powerful tool for studying human brain function due to its noninvasiveness and high spatial and temporal resolution[1—4]. Human brain adheres to two fundamental principles of functional organization, e.g. functional integration and functional specialization[5]. These principles indicate that organization of brain function varies on different spatial scales. On a large scale, a complex function may involve many specialized areas whose union is mediated by functional integration among them. Inversely, a single specialized area may respond to many different cognitive states, and the activity in that area is represented as distinctly distributed patterns for different stimulus on finer scales[6—12]. With the development of fMRI technology, the spatial resolution of a voxel in 2 mm width can be robustly achieved with standard clinical MRI scanners at 3T field strength. Using super high field strengths ($\geqslant$4 T), fMRI is invading the submillimeter range[13]. Such high spatial resolution of fMRI provides us the possibility to detect the fine-scale activity patterns evoked by the experimental stimulus[14, 15]. However, conventional univariate general linear model (GLM) analysis of fMRI data treats each voxel as a separate entity as far as statistical analysis is concerned[16]. It is lack of a mechanism to integrate the fine-scale information represented by the multi-voxel patterns. As a result, conventional univariate methods always fail to detect the fine-scale activity patterns of the experimental stimulus[17—19]. Additionally, univariate analysis heavily relies on spatial smoothing of the data with Gaussian kernel (GK) to increase the signal to noise and the statistical power[20]. Smoothing will obscure fine-scale patterns of weak effects that contain neuroscientifically relevant information. Consequently, an amount of information is removed by smoothing fMRI data and the high-resolution information that fMRI affords is not utilized[14, 15].

To distinguish the distinct brain activity patterns on fine scales and to efficiently use the spatial pattern information in the local brain regions, in this paper, a local multivariate distance mapping (LMDM) technique is proposed to extract the patterns of fMRI activation evoked by various experimental conditions. In contrast to the conventional univariate analysis,

* Supported by Cheung Kong Scholars Program and Innovative Research Team in University, National Program on Key Basic Research Projects (Grant No. 2006CB705700), Joint Research Fund for Overseas Chinese Young Scholars (Grant No. 30528027), National Natural Science Foundation of China (Grant Nos. 30600151, 30500131 and 60532050), and Natural Science Foundation of Beijing (Grant Nos. 4051002 and 4071003)

** To whom correspondence should be addressed. E-mail: tian@ieee.org

LMDM represents the effects elicited by the experimental stimulus with the multi-voxel patterns, and it employs multivariate distance between different activity patterns to map brain function. The local activity patterns contain more information than any voxel in the local regions. Therefore, using multivariate distance as the statistic can highlight fine-scale brain activation and extract the full spatial pattern of brain activity.

1 General description of LMDM

After the preprocessing steps (slice timing, spatial realignment, detrending, no spatial smoothing, and removing nonbrain voxels), fMRI data can be analyzed with LMDM as follows:

(i) For a specific voxel v_0 in the brain, a local region $N(v_0)$ containing k voxels is grouped by a region growing algorithm which adopts v_0 as the seed[21,22]. Region growing algorithm rather than a fixed regular window is used to find the local homogeneous regions, because the activity regions are always irregular. Region growing can well adapt the shape of the local spatial patterns structure of brain activity.

(ii) Assuming that the spatial patterns of the k voxels within the local region $N(v_0)$ evoked by various experimental conditions are sampled from different multivariate random variables, multivariate distance function derived from pattern classification technique is used to measure dissimilarity between different patterns.

(iii) The multivariate distance between the different patterns is assigned as the statistic at voxel v_0. It reveals the separability between different brain states by the activity patterns in local region $N(v_0)$. When $N(v_0)$ moves throughout the brain, multivariate distance statistic is computed for each voxel, and a continuous local multivariate distance map is constructed.

(iv) Nonparametric permutation test is performed to obtain the significant patterns to distinguish different experimental conditions[23,24].

2 Details of the LMDM technique

2.1 Multivariate statistical distance between multi-voxels patterns

Based on the experimental paradigm, multi-voxel patterns of the local regions measured in conditions A and B can be regarded as the data sampling from multivariate variable $\boldsymbol{X}_a = (X_{a1}, X_{a2}, \cdots, X_{ai}, \cdots, X_{ak})$ and $\boldsymbol{X}_b = (X_{b1}, X_{b2}, \cdots, X_{bi}, \cdots, X_{bk})$, respectively, where i stands for the index of the voxels in local region $N(v_0)$. Thus, multivariate statistical distance, such as Fisher linear discrimination function (FLDF) from Fisher linear discrimination analysis (FLDA)[25—27], maximal margin function (MMF) from support vector machine (SVM)[28], and other distance function[29], can be employed to quantify the degree of separation between the response patterns $\boldsymbol{X}_a$ and $\boldsymbol{X}_b$. For convenience, but without loss of generality, we use the FLDF to instantiate the LMDM method. As illustrated in Fig. 1, FLDA projects data from k dimensions of space onto the discriminant axis for the best separation of two datasets. FLDF statistic indicates the distance or separability of the two sets on the discriminant axis.

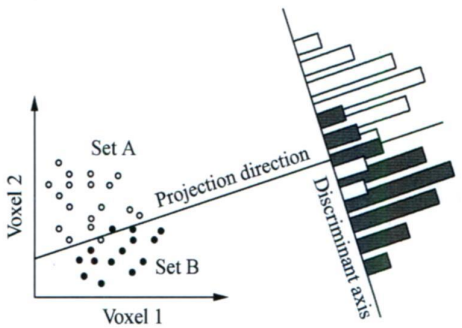

Fig. 1. FLDA projection of class samples onto the optimal discriminant axis. For visualization, only the first two dimensions (two-voxels pattern) are shown (empty circle and filled circle indicating the two datasets from conditions A and B, respectively).

The measurements from conditions A and B can construct two sample clusters $\boldsymbol{X}_a(n_a \times k)$ and $\boldsymbol{X}_b(n_b \times k)$, where n_a and n_b indicate the number of samples in conditions A and B, respectively.

FLDA determines the distance between two multivariate clusters relative to the intracluster variance. This distance is a function of the mean vector $\boldsymbol{d}$:

$$\boldsymbol{d} = \boldsymbol{X}_a - \boldsymbol{X}_b$$

where $\boldsymbol{X}_a$ and $\boldsymbol{X}_b$ are the mean vector for the cluster $\boldsymbol{X}_a$ and $\boldsymbol{X}_b$, respectively.

$$\boldsymbol{X}_a' = \frac{1}{n_a}\sum_{j=1}^{n_a} \boldsymbol{X}_a(j, \circ)$$

where $\boldsymbol{X}_a(j, \circ)$ represents the jth row of matrix $\boldsymbol{X}_a$, $\circ$ indicates all the columns (variables), and $\boldsymbol{X}_a'$ is the transpose of $\boldsymbol{X}_a$.

Denote the FLDF test statistic z as

$$z = \max_{\boldsymbol{a}_i}\left(\frac{\boldsymbol{a}_i'\boldsymbol{B}\boldsymbol{a}_i}{\boldsymbol{a}_i'\boldsymbol{W}\boldsymbol{a}_i}\right) \tag{1}$$

where $\boldsymbol{a}_i$ is the normalized column vector with length k, $\boldsymbol{B}$ and $\boldsymbol{W}$ are the between- and within-cluster sums of squares matrices, respectively. Specifically,

$$\boldsymbol{B} = \frac{n_1 n_2}{n_1 + n_2}\boldsymbol{d}\boldsymbol{d}'$$

$$\boldsymbol{W} = (n_1 + n_2 - 2)\boldsymbol{S}_{\mathrm{p}}$$

Here, $\boldsymbol{S}_{\mathrm{p}}$ is the pooled covariance matrix for $\boldsymbol{X}_{\mathrm{a}}$ and $\boldsymbol{X}_{\mathrm{b}}$:

$$\boldsymbol{S}_{\mathrm{p}} = \frac{(n_{\mathrm{a}} - 1)\boldsymbol{S}_{\mathrm{a}} + (n_{\mathrm{b}} - 1)\boldsymbol{S}_{\mathrm{b}}}{n_{\mathrm{a}} + n_{\mathrm{b}} - 2}$$

where $\boldsymbol{S}_{\mathrm{a}}$ represents the sample covariance matrix for the data matrix $\boldsymbol{X}_{\mathrm{a}}$:

$$\boldsymbol{S}_{\mathrm{a}} = \frac{1}{n_{\mathrm{a}} - 1}\sum_{j=1}^{n_{\mathrm{a}}}(\boldsymbol{X}_{\mathrm{a}}(j, \circ)' - \boldsymbol{X}_{\mathrm{a}})(\boldsymbol{X}_{\mathrm{a}}(j, \circ)' - \boldsymbol{X}_{\mathrm{a}})'$$

It can be proved that z is maximized when $\boldsymbol{a}_i$ equals $\boldsymbol{a}$, the first normalized eigenvector of $\boldsymbol{W}^{-1}\boldsymbol{B}$.

In the case of two groups, $\boldsymbol{a}$ is expressed as

$$\boldsymbol{a} = \frac{\boldsymbol{S}_{\mathrm{p}}^{-1}\boldsymbol{d}}{\| \boldsymbol{S}_{\mathrm{p}}^{-1}\boldsymbol{d} \|} \tag{2}$$

where $\boldsymbol{S}_{\mathrm{p}}^{-1}$ is the inverse of the pooled covariance matrix, and

$$\| \boldsymbol{S}_{\mathrm{p}}^{-1}\boldsymbol{d} \| = \sqrt{(\boldsymbol{S}_{\mathrm{p}}^{-1}\boldsymbol{d})'(\boldsymbol{S}_{\mathrm{p}}^{-1}\boldsymbol{d})}$$

Consequently, the test statistic can be expressed as

$$z = \frac{\boldsymbol{a}'\boldsymbol{B}\boldsymbol{a}}{\boldsymbol{a}'\boldsymbol{W}\boldsymbol{a}}$$

and can also be written as

$$z = c_{\mathrm{n}}(\boldsymbol{d}'\boldsymbol{S}_{\mathrm{p}}^{-1}\boldsymbol{d})$$

$$c_{\mathrm{n}} = \frac{(n_{\mathrm{a}} n_{\mathrm{b}})}{[(n_{\mathrm{a}} + n_{\mathrm{b}})(n_{\mathrm{a}} + n_{\mathrm{b}} - 2)]} \tag{3}$$

Since c_{n} is a function of the sample size only, it can be omitted, and so we can obtain

$$z = \boldsymbol{d}'\boldsymbol{S}_{\mathrm{p}}^{-1}\boldsymbol{d} \tag{4}$$

From Eq. (4), we can see that FLDF is equal to Mahalanobis distance in the two class situation.

The key of LMDM method is to use the multivariate distance function from pattern classification technique to measure the separability between different brain activity patterns. As alternatives to FLDF, maximal margin function (MMF) from support vector machine (SVM)[28] and other multivariate distance functions[29] can be easily incorporated into LMDM framework.

2.2 Statistic inference

Nonparametric permutation test is applied to calculate a map of p values for the local multivariate distance statistic. Here, the permutation test is more attractive than parameter test because its validity is independent of the multivariate distribution of the data[23, 24]. fMRI data is resampled in such a way that the spatial patterns of the data are unaltered, but their temporal sequence is randomly permuted repeatedly. This permutation destroys the correlation between fMRI signal and the experimental conditions, but keeps the spatial structure intact so that it can be used to determine the p maps corresponding to the distance between different experimental conditions. 1000 independent permutation realizations were performed. To obtain an inferential map accounting for multiple comparisons, the p map from randomization was thresholded to ensure that the average FDR was less than $q = 0.05$[30, 31].

3 Experiments and results

3.1 Simulated data

A two conditions event-related experiment was simulated. Each event lasted 500 ms and their onsets were separated by 16 s. The condition order was random, and there were 30 events per condition. The time course of fMRI signal associated with each condition was simulated by convolving each event to the canonical hemodynamic response function (HRF)[32]. The parameters of the functional volume are as follows: number of slice = 5, voxel sizes = 3 × 3 × 3 mm^3, TR = 2000 ms and matrix = 64 × 64. Five active regions with different shapes and varied sizes (10, 30, 90, 180 and 270 voxels, respectively) were generated. Each condition was associated with a Gaussian white-noise effect pattern within the active regions and no effects outside the regions. Taking Gaussian white-noises as the effect patterns ensured the effect power distributed among all the spatial-frequency bands. Consequently, the condition information was contained both in their locally averaged components (low frequency) and in their spatial fine structures (high frequency). The effect signals were added to the spatiotemporal noise generated by slight spatial smoothing of Gaussian white noise with a GK of 3.5 mm full width at half maximum (FWHM) to

imitate the correlation found between the residual time courses of neighboring voxels in real fMRI data. Five datasets were generated with different functional contrast-to-noise ratio (CNR) levels (0.2, 0.4, 0.6, 0.8, and 1.0). The CNR was defined as the spatial average within the effect region of the absolute activity level at the maximum of the hemodynamic response divided by the temporal standard deviation of the background noise[33].

3.2 Simulated data analysis

The simulated data were analyzed in three ways: GLM with no smoothing (GLM), GLM with GK (GK-GLM), and LMDM method. Two GK with FWHM of 6 mm and 9 mm were applied separately to smooth the data. There were two widely used GK in fMRI data analysis. For comparison, two local regions with 10 and 30 voxels were adopted in LMDM technique to approximatively match the range of spatial combination of signals between GK-GLM and LMDM approaches.

Receiver operating characteristic (ROC) analysis was conducted on the simulated data for quantitative evaluation of three different analyses[34, 35]. An ROC curve is the plot of true activation rate versus false activation rate for the threshold varying over the complete range of map values.

True activation rate (sensitivity) is the ratio of the number of voxels correctly identified as activation to the total number of truly activated voxels.

False activation rate (1-specificity) is the ratio of the number of voxels incorrectly identified as activation to the total number of truly non-activated voxels.

ROC shows the tradeoff relationship between sensitivity and specificity of the activation detection methods. Thus, it provides a way to compare the performance of different analyses quantitatively. Furthermore, the area under ROC (AUC) represents a summary measure of what extent of high sensitivity and specificity can be simultaneously achieved. Concretely, AUC indicates how well a given statistic distinguishes effect regions from pure noise in our simulations.

Fig. 2 shows the AUC for each analysis plotted as functions of CNR. It is clear that smoothing degrades performance of the GK-GLM under every CNR. The more smoothing, the worse the performance is, because GK smoothing fails to benefit from local spatial combination of signals. LMDM performs much better than GLM and GK-GLM for all situations, benefiting from spatial multivariate representation of signals within the local region.

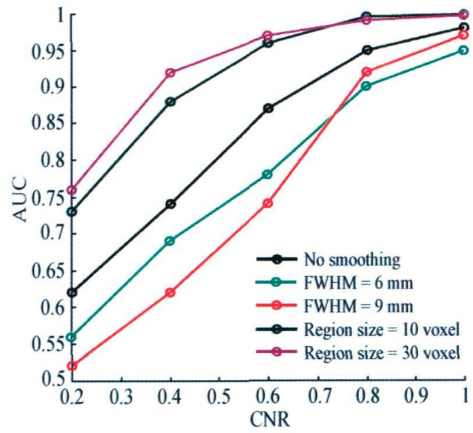

Fig. 2. Area under ROC for GLM, GK-GLM and LMDM at various CNR, averaged over 30 simulations.

Fig. 3 illustrates the ROC curves of different analyses for one particular case of the simulated data with CNR being 0.6. It can be observed that the ROC curves of LMDM approached the top left corner primely, and above the curves of GLM and GK-GLM. This further clarifies the increased sensitivity of the LMDM. With no smoothing, GLM performs worse than LMDM, but better than GK-GLM. This reflects the fact that effects in our simulation are equally strong in all spatial-frequency bands up to the Nyquist limit imposed by voxel size. GK-GLM can not detect the high frequency fine-scale patterns because GK has filtered out the high spatial-frequency component of the effect patterns. However, LMDM can effectively employ the local distributed spatial patterns in all frequency components to discriminate the effect under different conditions.

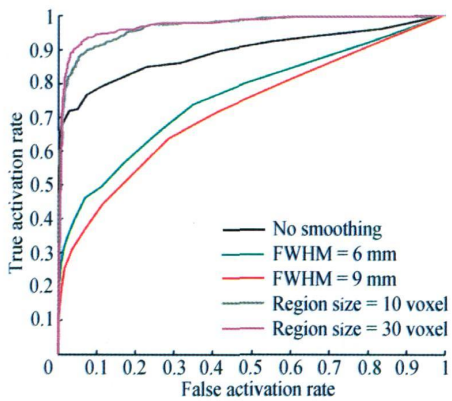

Fig. 3. ROC curves for one special case of simulated data with CNR being 0.6.

To gain an intuitive understanding of the quantitative ROC results, Fig. 4 illustrates the unthresholded maps from the GLM, GK-GLM and LMDM analyses at CNR being 0.6. The absolutely t map obtained by GLM performed on unsmoothed data did not highlight the effect regions accurately, and the SNR of the map was low. When the same map was computed from GK-GLM with FWHM being 9 mm, some correct hot spots remained, but many incorrect ones appeared outside the effect regions. Clearly, smoothing degraded the sensitivity of GK-GLM analysis since it removed the information in the high-spatial-frequency band of the effects. In contrast, LMDM with local region size of 30 voxels provided a much better map, which correctly highlighted the effect regions. This indicates that the LMDM technique properly integrates the adjacent subtle effects in the local regions and improves the power in discriminating the brain activity patterns evoked by different conditions.

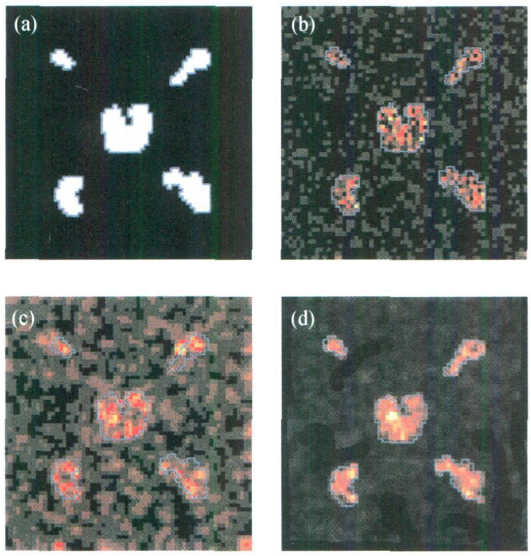

Fig. 4. The unthresholded maps obtained with GLM, GK-GLM and LMDM analyses for one particular case of the simulated fMRI data at CNR being 0.6. (a) Results of GLM; (b) results of GK-GLM with FWHM being 9 mm; (c) results of LMDM with local region size of 30 voxels.

3.3 Real fMRI data

A block design experiment with two conditions (face and house) was employed. Six subjects were presented with pictures of human faces or houses for each condition. Subjects continuously fixated on a central cross while viewing images. There were 6 face blocks and 6 house blocks in total. Each block contained 20 images and each image was presented for 500 ms, the block lasted 30 s. There was a 1s crosshair fixation between each images. Baselines (crosshair fixation) last about 10s. BOLD fMRI data were acquired with a T2*-weighted gradient echo EPI sequence: TR = 2000 ms, TE = 30 ms, FOV = 240×240 mm^2, matrix = 64×64, number of slices = 25, and slice thickness = 4 mm.

All data were preprocessed using SPM2 (http://www.fil.ion.ucl.ac.uk/SPM/)[16] as follows: Slices were temporally realigned to compensate for the acquisition time lag. Whole volume images were realigned to compensate for the head movement, and drifts were corrected by second-order polynomial detrending. For LMDM analysis, time series were shifted 4 s forwards to offset the time delay of HRF. In addition, volumes acquired during transitions between experimental states were removed. Such volume removal simplified experimental state assignments and further reduced HRF effects.

3.4 Real fMRI data analysis

After being preprocessed, fMRI data were analyzed using GLM, GK-GLM and LMDM. As seen from the simulation experiment, LMDM performed better when the local region size was 30 voxels. We hereby set the local region size as 30 voxels in the analysis of real fMRI data. A GK of FWHM being 9 mm was used in the GK-GLM analysis to approximately match the range of spatial combination of signals between LMDM and GK-GLM analyses.

As illustrated in Fig. 5, all the three analyses found the major blobs of brain activity (FFA: fusiform face area; PPA: parahippocampal place area) evoked by the experimental conditions[9, 10, 12, 36, 37]. The GLM and GK-GLM analyses detected the voxels which are more strongly active during face perception than house perception and *vice versa*, whereas LMDM highlighted regions whose local activity pattern distinguished the face and house conditions. It can be observed that GLM analysis could roughly localize the activated region, whereas the activation maps show salt-and-pepper phenomenon seriously (Fig. 5(a)). GK-GLM with FWHM being 9 mm resulted in the clean maps, and only voxels that responded maximally to the category being viewed were retained (Fig. 5(b)). In contrast, as shown in Fig. 5(c), LMDM with local regions containing 30 voxels that closely matched the size of GK of FWHM being 9 mm was able to better

detect the activated voxels whether its response to the category being viewed was strong or weak, suggesting that the representations of faces and house extended beyond the foci regions detected by GK-GLM. This indicates that there are many voxels containing the effects related to the experimental conditions in the fine-grained structure of the activity patterns. GK-GLM failed to detect these regions because the specific information was lost when the data were smoothed.

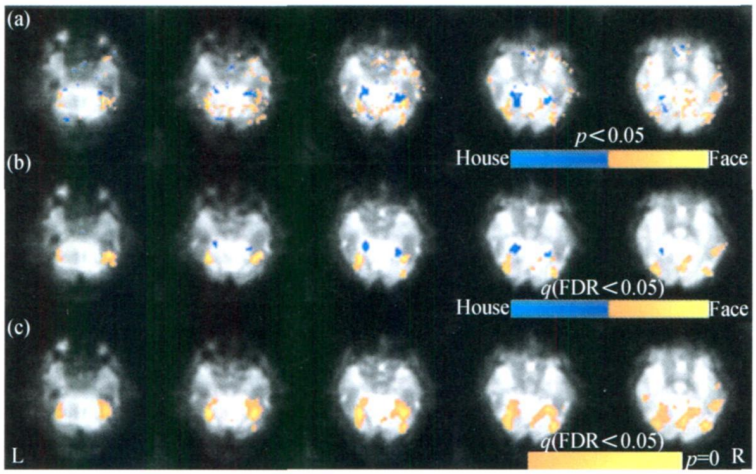

Fig. 5. Activation maps of real fMRI data (face vs house). (a) Results of GLM; (b) results of GK-GLM with FWHM being 9 mm; (c) results of LMDM with local region size of 30 voxels. L: left; R: right.

We further found that among the subjects, all activation regions detected by LMDM were distributed more widely than that detected by the GLM. To measure the reproducibility of statistical maps from each of the three analyses, we transformed all statistical parameter maps to the MNI template, and calculated the pairwise correlation coefficients (r) of the $C_6^2(15)$ pairs of maps from the identical method. The intersubject correlation coefficients for each analysis were summarized by its mean and standard errors of the mean ($\bar{r} \pm \mathrm{sem}$) as shown in Fig. 6. Clearly, the reproducibility of the maps from GLM (0.25 ± 0.04) is the lowest in the three analyses. The unsmoothed fMRI maps were very noisy, so the reproducibility of it is very low. The reproducibility of the maps from LMDM (0.49 ± 0.03) is somewhat lower than that from GK-GLM (0.57 ± 0.02). This is mainly because activity patterns are unique to each individual on the fine spatial scale of millimeters. Therefore, multi-subject group averaging on fine scale is a challenging issue, and further investigation is needed.

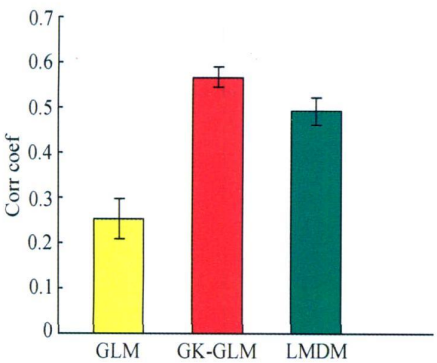

Fig. 6. The reproducibility of the activation maps from each analysis.

4 Discussion

fMRI data contain wealthy information of brain activity from coarse scale to fine scale. Currently, few efforts have been focused directly on extracting the fine-grained information hidden in fMRI data. Conventional univariate analysis of fMRI data relies exclusively on the information contained in the time course of individual voxels, and the preprocessing procedure also inappropriately removes some fine-scale information. In this paper, we have proposed a local multivariate distance mapping technique to map the brain function. By combining multi-voxel pattern information within the local homogenous region, LMDM is sensitive to the spatial fine structure, and can efficiently distinguish the representation of various brain states. Results from the simulation and real fMRI data demonstrate that LMDM method has better performance to detect the fine-scale spatial patterns of brain activation.

References

1 Kwong KK, Belliveau JW, Chesler DA, et al. Dynamic magnetic resonance imaging of human brain activity during primary sensory stimulation. Proceedings of the National Academy of Sciences USA, 1992, 89(12): 5675—5679

2 Ogawa S, Lee TM, Kay AR, et al. Brain magnetic resonance imaging with contrast dependent on blood oxygenation. Proceedings of the National Academy of Sciences USA, 1990, 87(24): 9868—9872

3 Logothetis NK, Pauls J, Augath M, et al. Neurophysiological investigation of the basis of the fMRI signal. Nature, 2001, 412(6843): 150—157

4 Raichle ME and Mintun MA. Brain work and brain imaging. Annual Review of Neuroscience, 2006, 29: 449—476

5 Frackowiak RSJ, Ashburner JT, Penny WD, et al. Human Brain Function, 2nd ed. San Diego: Academic Press, 2003, 971—1118

6 Haynes JD and Rees G. Decoding mental states from brain activity in humans. Nature Review Neuroscience, 2006, 7(7): 523—534

7 Cohen JD and Tong F. The face of controversy. Science, 2001, 293(5539): 2405—2407

8 Boynton GM. Imaging orientation selectivity: decoding conscious perception in V1. Nature Neuroscience, 2005, 8(5): 541—542

9 Haxby JV, Gobbini MI, Furey ML, et al. Distributed and overlapping representations of faces and objects in ventral temporal cortex. Science, 2001, 293(5539): 2425—2430

10 Carlson TA, Schrater P and He S. Patterns of activity in the categorical representation of objects. Journal of Cognitive Neuroscience, 2003, 15(5): 704—717

11 Kamitani Y and Tong F. Decoding the visual and subjective contents of the human brain. Nature Neuroscience, 2005, 8(5): 679—685

12 O'Toole A, Jiang F, Abdi H, et al. Partially distributed representation of objects and faces in ventral temporal cortex. Journal of Cognitive Neuroscience, 2005, 17(4): 580—590

13 Harel N, Ugurbil K, Uludag K, et al. Frontiers of brain mapping using MRI. Journal of Magnetic Resonance Imaging, 2006, 23(6): 945—957

14 Kriegeskorte N, Goebel R and Bandettini P. Information-based functional brain mapping. Proceedings of the National Academy of Sciences USA, 2006, 103(10): 3863—3868

15 Bandettini P. Functional MRI today. International Journal of Psychophysiology, 2007, 63(2): 138—145

16 Friston KJ, Holmes AP, Worsley KJ, et al. Statistical parametric maps in functional imaging: a general linear approach. Human Brain Mapping, 1995, 2(4): 189—210

17 Petersson KM, Nichols T, Poline JB, et al. Statistical limitations in functional neuroimaging I. Non-inferential methods and statistical models. Philosophical Transactions of the Royal Society of London B, 1999, 354(1387): 1240—1260

18 Petersson KM, Nichols T, Poline JB, et al. Statistical limitations in functional neuroimaging II. Signal detection and statistical inference. Philosophical Transactions of the Royal Society of London B, 1999, 354(1387): 1261—1281

19 Tian J, Yang L and Hu J. Recent advances in the data analysis method of functional magnetic resonance imaging and its applications in neuroimaging. Progress in Natural Science, 2006, 16(8): 785—795

20 Friston KJ, Josephs O, Zarahn E, et al. To smooth or not to smooth? Bias and efficiency in fMRI time-series analysis. NeuroImage, 2000, 12(2): 196—208

21 Bellec P, Perlbarg V, Jbabdi S, et al. Identification of large-scale networks in the brain using fMRI. NeuroImage, 2006, 29(4): 1231—1243

22 Lu Y, Jiang T and Zang Y. Region growing method for the analysis of functional MRI data. NeuroImage, 2003, 20(1): 455—465

23 Efron B and Tibshirani R. An Introduction to the Bootstrap. New York: Chapman & Hall, 1993, 202—219

24 Nichols TE and Holmes AP. Nonparametric permutation tests for functional neuroimaging: a primer with examples. Human Brain Mapping, 2002, 15(1): 1—25

25 Mardia K, Kent J and Bibby J. Multivariate Analysis. London: Academic Press, 1979, 300—332

26 Johnson R and Wichern D. Applied Multivariate Statistical Analysis. 5th ed. Englewood Cliffs, New Jersey: Prentice-Hall, 2002, 581—667

27 Duda RO, Hart PE and Stork DG. Pattern Classification. 2nd ed. New York: Wiley-Interscience, 2000, 215—281

28 Vapnik VN. Statistical Learning Theory. New York: Wiley-Interscience, 1998, 401—520

29 Zhou SK and Chellappa R. From sample similarity to ensemble similarity: probabilistic distance measures in reproducing kernel Hilbert space. IEEE Transactions on Pattern Analysis and Machine Intelligence, 2006, 28(6): 917—929

30 Benjamini Y and Yekutieli D. The control of the false discovery rate in multiple testing under dependency. The Annals of Statistics, 2001, 29(4): 1165—1188

31 Genovese CR, Lazar NA and Nichols TE. Thresholding of statistical maps in functional neuroimaging using the false discovery rate. NeuroImage, 2002, 15(4): 870—878

32 Friston KJ, Fletcher P, Josephs O, et al. Event-related fMRI: characterizing differential responses. NeuroImage, 1998, 7(1): 30—40

33 Langer N. Tutorial in biostatistics: statistical approaches to human brain mapping by functional magnetic resonance imaging. Statistics in Medicine, 1996, 15(4): 389—428

34 Sorenson J and Wang X. ROC methods for evaluation of fMRI techniques. Magnetic Resonance in Medicine, 1996, 36(5): 737—744

35 Skudlarski P, Constable RT and Gore JC. ROC analysis of statistical methods used in functional MRI: individual subjects. NeuroImage, 1999, 9(3): 311—329

36 Kanwisher N, McDermott J and Chun MM. The fusiform face area: A module in human extrastriate cortex specialized for face perception. The Journal of Neuroscience, 1997, 17(11): 4302—4311

37 Kanwisher N and Yovel G. The fusiform face area: a cortical region specialized for the perception of faces. Philosophical Transactions of the Royal Society of London B, 2006, 361(1476): 2109—2128